Indonesian Journal of Chemical Research

http://ojs3.unpatti.ac.id/index.php/ijcr Indo. J. Chem. Res., 12 (1), 31-39, 2024

Structural and Molecular Dynamics Investigation of Bacterial and Fungal Xylanases

Noer Komari[1,2*], Rahmat Eko Sanjaya[1,2], Andifa Anugerah Putra[2], Amaris Nathania Hanindia Putri[1], Nur Fatma Febriyanti[1]

[1]Department of Chemistry, Faculty of Mathematics and Natural Sciences, Universitas Lambung Mangkurat, Jalan A. Yani KM 36, Banjarbaru 70714, South Borneo, Indonesia

[2]Bioinformatics Laboratory, Integrated Laboratory, Universitas Lambung Mangkurat, Jalan A. Yani KM 36, Banjarbaru 70714, South Borneo, Indonesia

[*]*Corresponding Author: nkomari@ulm.ac.id*

Received: December 2023
Received in revised: April 2024
Accepted: May 2024
Available online: May 2024

Abstract

Xylanase is a type of enzyme that hydrolyzed of β-1,4 glycosidic bonds in xylan, breaking it down into its constituent monomers. Xylanolytic enzymes are pivotal in processes such as bio-bleaching of pulp, textile manufacturing, and the recycling of waste paper. Successful bioconversion of xylan or lignocellulose relies on the collaborative action of various xylanolytic enzymes, including endo-xylanase, β-xylosidase, and other accessory enzymes. Docking simulations using Auto Dock 4.2 were conducted to analyze the interaction between ligands and xylanase, utilizing PDB 1B3V and 1FCE. Ligand interaction with xylanase was further investigated through molecular dynamics. The xylanase from *Penicillium simplicissimum* (PDB 1B3V) exhibited comparable affinities for α-D-xylopyranose and β-D-xylopyranose. In contrast, the xylanase from *Clostridium cellulolyticum* (PDB 1FCE) demonstrated a stronger affinity for β-D-glucopyranose than for 4-thiouridine. Molecular dynamic investigations indicated the stability of both structures against the tested ligands. These findings provide a foundation for potential experimental validations and the application of molecular mechanics techniques. Such approaches could unveil the detailed catalytic mechanism and bolster the industrial efficacy of the enzyme.

Keywords: molecular docking, molecular dynamic, xylanase, ligand

INTRODUCTION

Xylanase, type of enzymes that catalyze the hydrolysis reaction of β-1,4 glycosidic bonds from xylan into its monomers. The xylanolytic enzyme consisted of endo-β-1,4-xylanase, β-xylosidase, and several other enzymes, such as α-L-arabinofuranosidase, α-glucuronidase, acetyl xylan esterase, ferulic acid esterase, and p-coumaric acid esterase (Saha, 2003). Each of these enzymes has a specific role in xylan degradation. The xylanase enzyme can degrade lignocellulosic waste, especially hemicellulose, into useful products such as prebiotics, bioethanol, animal feed, and xylitol, as well as other fermentation products which are widely used by the industry (Wong et al., 1988).

Xylanolytic enzymes are produced extracellularly by fungi and bacteria. *Aspergillus* spp and *Trichoderma* spp produce extracellular xylanase(Dos Reis et al., 2003; Nair & Shashidhar, 2008; Polizeli et al., 2005; Rusli et al., 2009). Extracellular xylanase secreted by *Penicillium janczewskii* has been successfully applied in the pulp bio bleaching process (Terrasan et al., 2013). Extracellular xylanases from fungi were successfully cloned and expressed intracellularly in *E. coli* (Bhalla et al., 2014; Rashid et al., 2020) and extracellularly in *Saccharomyces cerevisiae* (Den Haan & Van Zyl, 2003). Bacteria from the genus *Bacillus* are one of the genera that secrete xylanase extracellularly and have been widely explored (Safitri et al., 2021).

Xylanolytic enzymes play a crucial role in bio-bleaching pulp, processing textiles, and recycling waste paper. Biomass derived from agricultural waste can serve as a valuable raw material for paper and textile production, as well as for the formulation of animal feed and bioethanol (Annadurai et al., 2021; Javed et al., 2017; Patel et al., 2019). Paper and pulp industry relies on chlorine compounds for lignin removal, a process known as bio-bleaching. However, the use of chlorine as a bleaching agent poses significant environmental concerns, necessitating the exploration of more eco-friendly and efficient

alternatives. The utilization of xylanolytic enzymes in paper bleaching has proven to be successful, providing satisfactory results in the bleaching process (Parab & Khandeparker, 2021; Ramos et al., 2022). This approach offers a more environmentally friendly and effective solution, addressing the negative impacts associated with chlorine-based bleaching methods.

The bioconversion of xylan or lignocellulose necessitates the collaboration of various xylanolytic enzymes, including endo-xylanase, β-xylosidase, and other accessory enzymes. Fermentation products derived from the bioconversion of xylan include xylitol. Xylitol possesses pharmacological properties that can help prevent tooth decay and ear infections in children (Polizeli et al., 2005; Swain & Krishnan, 2015), making it a valuable ingredient in toothpaste and food sweeteners. The xylose fermentation byproduct also includes 2,3-butanediol, a compound serving as a raw material for organic solvents, fuels, and polymer precursors. Further dehydration of 2,3-butanediol yields 1,3-butanedione, a crucial starting material in rubber manufacturing and an important monomer in the polymer industry.

Computational approaches using docking and molecular dynamics provide new insights into the knowledge of protein structure and its interactions. Several studies have employed docking and other computational methodologies to address various challenges, such as drug discovery and identifying ligands that interact with receptors (Danova et al., 2023; Fitriana & Royani, 2022; Gaspersz & Sohilait, 2019; Mulyati & Seulina Panjaitan, 2021). Knowledge of binding positions and substrate interactions with the highly thermostable GH10 Xylanase from *Thermotoga maritima* was obtained through computational approaches using AutoDock tools (Yang & Han, 2018). The interaction of six thermoacidophilic GH11 xylanases from various fungal species (*Gymnopus androsaceus*, *Penicilliopsis zonata*, *Aspergillus neoniger*, *Calocera viscosa*, *Acidomyces richmondensis*, *Oidiodendron maius)* with substrates can be determined through computational approaches (Sürmelı, 2023). Docking also aids in identifying the amino acids involved in interactions with ligands in xylanase from *Bacillus bravis*, as revealed through computational approaches (Mathur et al., 2017). This underscores the important role of docking in studying enzyme structures and their interactions with ligands.

In this study, the structure of xylanase from fungal, *Penicillium simplicissimum* and bacterial, *Clostridium cellulolyticum* has been determined, each possessing the PDB ID 1B3V and 1FCE, respectively. The structural analysis involved investigating enzyme-ligand interactions through molecular docking using Auto Dock. Additionally, molecular dynamics simulations were conducted to examine the structural dynamics resulting from interactions with ligands. The computational approaches employed in this study aimed to develop theoretical models for various bacterial and fungal xylanase enzymes. These models are anticipated to contribute to the enhancement of xylan-degrading efficiency in these enzymes, ultimately leading to increased bioethanol yield.

METHODOLOGY

Molecular Docking

The blind molecular docking simulations of ligands and xylanase with PDB 1B3V and 1FCE were conducted using AutoDock 4.2 with the Lamarckian Genetic Algorithm (LGA) to calculate possible ligand conformations bound to the protein. In this study, the following ligands (α-D-xylopyranose and β-D-xylopyranose for 1B3V, and 4-thiouridine and β-D-glucopyranose for 1FCE) were examined. The hydrogen bond interactions between the ligands and the receptor were analyzed using Discovery Studio Visualizer.

Molecular Dynamics

Molecular dynamics simulation was performed for 10 ns for the structure of 1B3V-ligand and 1FCE-ligand using Gromacs program (Abraham et al., 2015). This method enables the analysis of crucial parameters, including RMSD (Root Mean Square Deviation), RMSF (Root Mean Square Fluctuation), RG (Radius of Gyration), and SASA (Solvent Accessible Surface Area). The steps involved in conducting molecular dynamics encompass system preparation, force field selection, energy minimization, equilibration, simulation, and the subsequent analysis of RMSD, RMSF, Rg, and SASA.

RESULTS AND DISCUSSION

Two protein-ligand complexes were analyzed: 1B3V and 1FCE. The lowest binding energy and the amino acid interactions and distances between the protein and ligand were evaluated for each complex. For the first complex, 1B3V, the ligand used was α-D-xylopyranose (Figure 1a & 1b). The lowest binding energy observed was –5.6 kcal/mol. The interactions between the ligand and the amino acids in the protein were primarily through hydrogen bonds (Table 1). Specifically, Gln208 formed hydrogen bonds with the

ligand at distances of 2.02 Å and 2.96 Å, and Glu238 formed a hydrogen bond at 2.45 Å and 2.20 Å. For the second complex, 1FCE, two ligands were studied: 4-Thiouridine and β-D-glucopyranose (Figure 2). The lowest binding energy observed for 4-thiouridine was –5.7 kcal/mol. The ligand formed hydrogen bonds with several amino acids, including Trp154 (2.34 Å), Asn178 (2.58 Å), Gln181 (2.69 Å), Thr226 (2.24 Å), and Tyr403 (2.67 Å). Additionally, a *pi*-sulfur interaction was observed between the ligand and Tyr299 (4.25 Å). The lowest binding energy observed for β-D-glucopyranose was –5.9 kcal/mol. Like the previous complex, hydrogen bonds were formed between the ligand and specific amino acids, including Glu184 (3.04 Å and 3.47 Å), Thr375 (2.88 Å), Asn379 (2.06 Å), Val402 (2.39 Å and 2.47 Å), and Asn400 (2.64 Å). Additionally, a carbon-hydrogen bond interaction was observed between the ligand and His318 (3.31 Å). In summary, the outcomes of protein-ligand docking reveal the formation of stable complexes between 1B3V and 1FCE with their respective ligands. The remarkably low binding energies indicate favorable affinities between the proteins and ligands in each instance. The identified interactions, including hydrogen bonds and pi-sulfur interactions, are pivotal contributors to the stability of these complexes.

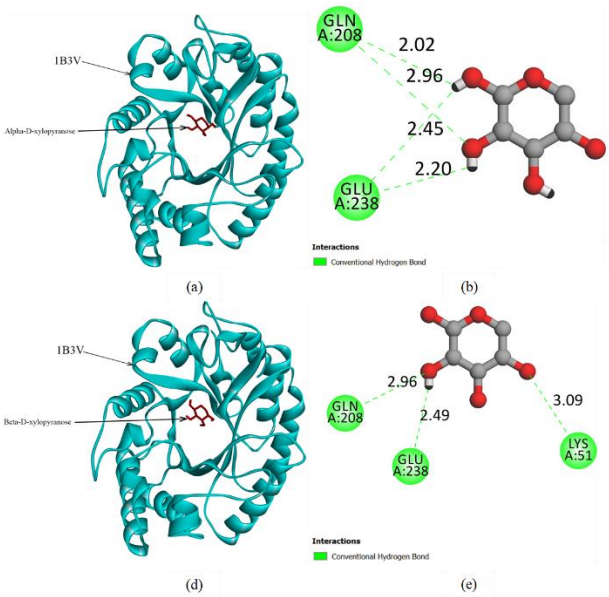

Figure 1. Molecular docking and ligand interaction of fungal xylanase from *Penicillium simplicissimum* (PDB 1B3V).

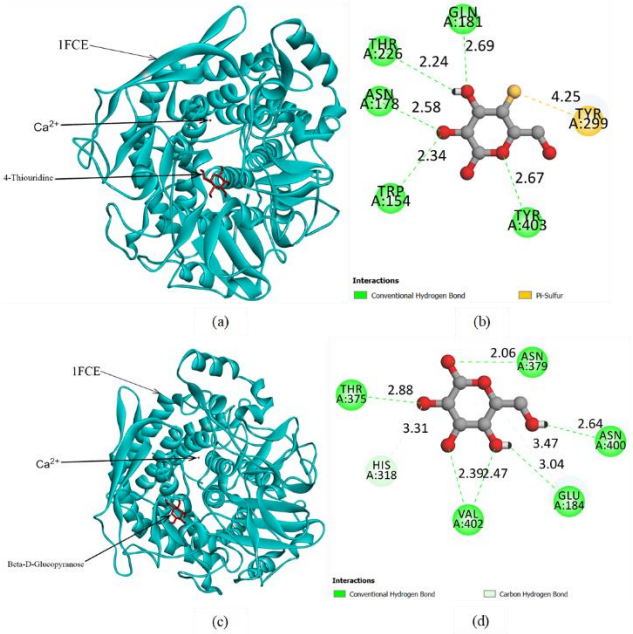

Figure 2. Molecular docking and ligand interaction of bacterial xylanase from *Clostridium cellulolyticum* (PDB 1FCE).

Flexibility, stability, conformational changes, and solvent accessibility were assessed through a molecular dynamics' investigation (Fu et al., 2018; Gyebi et al., 2021). By comparing these parameters across different systems or at various time points during the simulation, valuable insights can be gleaned regarding the behavior and dynamics of biomolecules and their interactions with ligands or other components. Root Mean Square Deviation (RMSD) serves as a widely utilized metric in molecular dynamics simulations for gauging structural similarity between a reference structure and a series of time-dependent structures. It measures the average displacement of atoms in the simulated system from their initial positions. The molecular dynamics simulation was conducted over a duration of 10 nanoseconds (ns).

Table 1. Binding energy, interactions, and residue-ligand distance resulting from the molecular docking of the protein-ligand complex.

Protein – Ligand	Lowest Binding Energy (kcal/mol)	Amino Acids Interaction and Distance
1B3V – α-D-xylopyranose	–5.6	*Hydrogen Bond* Gln208 (2.02, 2.96) Gln238 (2.45, 2.20)
1B3V – β-D-xylopyranose	–5.5	*Hydrogen Bond* Lys51 (3.09) Gln208 (2.96)

		Glu238 (2.49)
1FCE – 4-thiouridine	–5.7	*Hydrogen Bond* Trp154 (2.34) Asn178 (2.58) Gln181 (2.69) Thr226 (2.24) Tyr403 (2.67) *Pi-Sulfur* Tyr299 (4.25)
1FCE – β-D-glucopyranose	– 5.9	*Hydrogen Bond* Glu184 (3.04, 3.47) Thr375 (2.88) Asn379 (2.06) Val402 (2.39, 2.47) Asn400 (2.64) *Carbon Hydrogen Bond* His318 (3.31)

This implies that the simulation effectively captured the dynamic behavior of the system throughout a 10 ns timeframe, furnishing insights into the structural variations during this period. The RMSD values derived from the simulation can be scrutinized to comprehend the molecule's stability and conformational alterations. A diminished RMSD value signifies a closer alignment between structures at distinct time points, indicating a more consistently stable conformation throughout the simulation (Allen et al., 2015; Cole et al., 2005). Conversely, an elevated RMSD value implies more substantial structural deviations and potential conformational changes within the molecule. It is crucial to recognize that the interpretation of RMSD values is contingent upon the specific system and the simulation's context.

The comparison of RMSD derived from molecular dynamics simulations involving complexes 1FCE with 4-thiouridine and β-D-glucopyranose yields insights into their structural stability (Figure 3b). The mean value of the dependent variable (RMSD) for 4-thiouridine is 0.08540826, whereas for β-D-glucopyranose, it is 0.1144946. This implies that β-D-glucopyranose exhibits a slightly higher average RMSD, suggesting potentially greater structural fluctuations or flexibility in comparison to 4-thiouridine. Examination of the standard deviations reveals that 4-thiouridine has a standard deviation of 0.007272577, while β-D-glucopyranose has a standard deviation of 0.01871177. This suggests that β-D-glucopyranose displays greater variability in RMSD values, indicating heightened structural dynamics or potential conformational changes compared to 4-thiouridine.

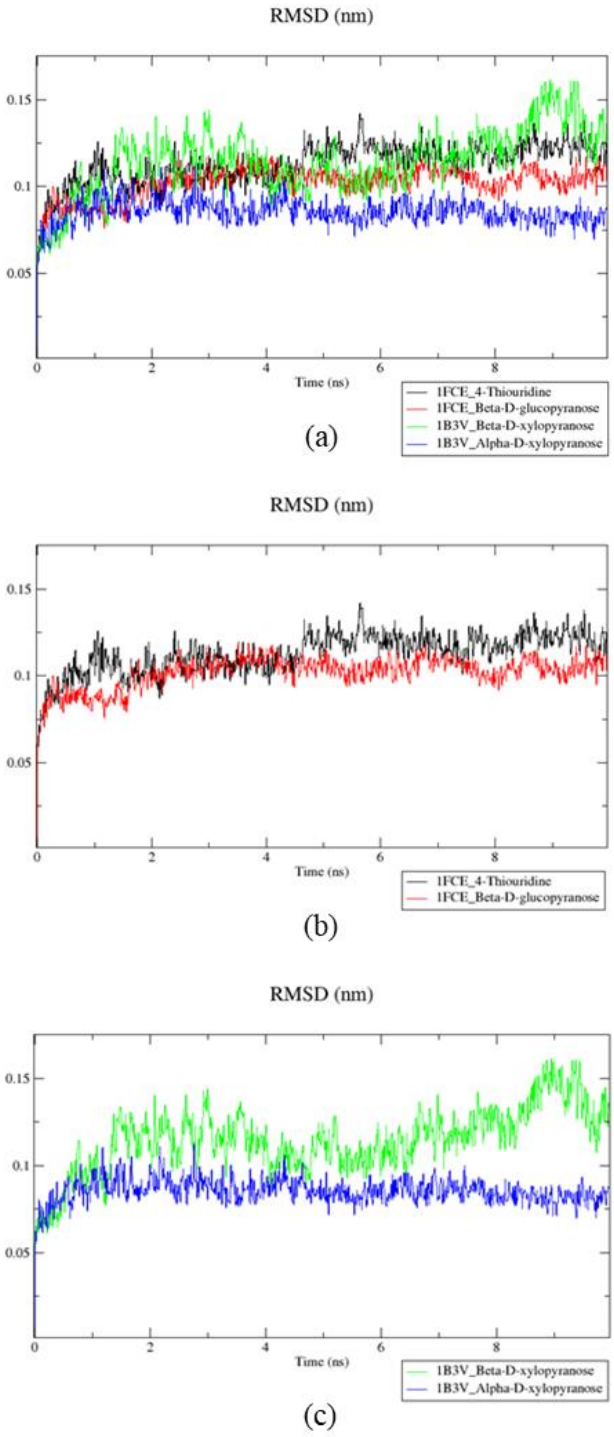

Figure 3. Root Mean Square Deviation (RMSD) of xylanase – ligand complexes.

The analysis of RMSD values from molecular dynamics simulations involving complex 1B3V with β-D-xylopyranose and α-D-xylopyranose sheds light on their structural stability (Figure 3c). The mean value of the dependent variable (RMSD) for β-D-xylopyranose is 0.1019471, whereas for α-D-xylopyranose, it is 0.1127125. This suggests that α-D-

xylopyranose displays a slightly higher average RMSD, indicating potentially more substantial structural fluctuations or flexibility when compared to β-D-xylopyranose. In the examination of standard deviations, β-D-xylopyranose has a standard deviation of 0.00939857, while α-D-xylopyranose has a standard deviation of 0.01181132. This points to α-D-xylopyranose exhibiting greater variability in RMSD values, signifying heightened structural dynamics or potential conformational changes compared to β-D-xylopyranose. The comparison of RMSD values between β-D-xylopyranose and α-D-xylopyranose in protein-ligand molecular dynamics simulations reveals that α-D-xylopyranose shows slightly higher average and more variable RMSD values, indicating greater structural fluctuations.

In molecular dynamics simulations, the root mean square (RMS) fluctuation serves as a metric for quantifying the average deviation or movement of atoms or particles within a system over time (Senthilkumar & Rajasekaran, 2017). This metric provides valuable insights into the dynamic behavior and stability of the system. When analyzing two variables, comparing their RMS fluctuations enables an understanding of their relative impacts on the overall system dynamics. This comparative assessment of RMS fluctuations between two variables allows for the evaluation of their respective magnitudes of fluctuation, offering insights into their contributions to the overall system dynamics. Such comparisons assist in identifying which variable may exert a more pronounced effect on the system's behavior and contribute to a more thorough analysis and interpretation of the molecular dynamics simulation results.

4-thiouridine exhibits a marginally higher mean for the dependent variable (0.06649078) compared to β-D-glucopyranose (0.06182846). This suggests that, on average, fluctuations in 4-thiouridine are slightly more pronounced than those in β-D-glucopyranose (Figure 4a). Further analysis of the standard deviations reveals a slightly elevated standard deviation for the dependent variable of 4-thiouridine (0.03122098) in comparison to β-D-glucopyranose (0.02622183). This implies that fluctuations in 4-thiouridine demonstrate slightly greater variability or dispersion than those in β-D-glucopyranose. The comparison of the two variables, β-D-xylopyranose and α-D-xylopyranose, based on the provided information on RMS fluctuation, unveils intriguing

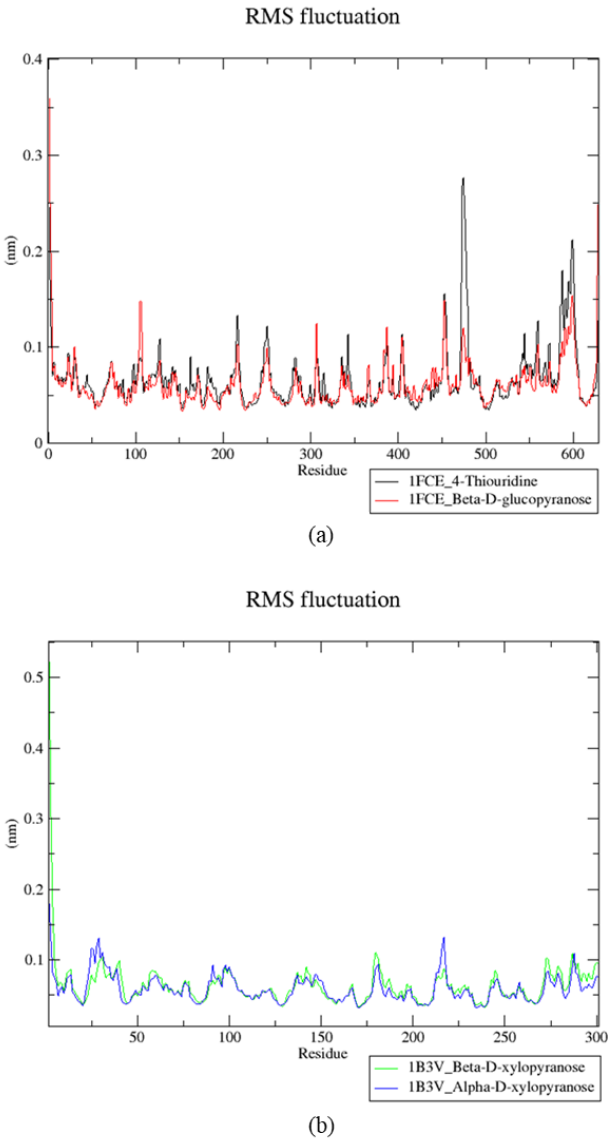

Figure 4. Root Mean Square Fluctuation (RMSF) of xylanase – ligand complexes.

insights (Figure 4b). In terms of mean values, β-D-xylopyranose exhibits a slightly higher average for the dependent variable (0.06383223) compared to α-D-xylopyranose (0.05944518), indicating somewhat larger fluctuations in β-D-xylopyranose, on average. In summary, the examination of β-D-xylopyranose and α-D-xylopyranose based on RMS fluctuation discloses that β-D-xylopyranose displays slightly more substantial fluctuations and a greater variability value compared to α-D-xylopyranose.

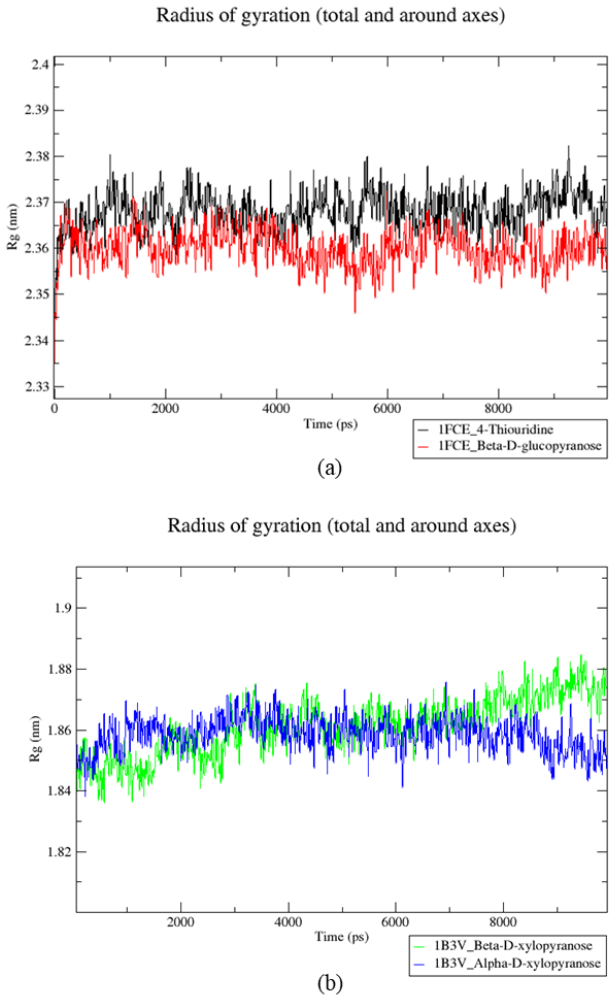

Figure 5. Radius of gyration (Rg) of xylanase – ligand complexes.

The Radius of Gyration (Rg) within molecular dynamics simulations serves as a metric offering insights into the overall dimensions, configuration, and compactness of a system. It derives from the positions of atoms or particles within the system, signifying the root mean square distance of these entities from their center of mass. A higher Rg value suggests a larger and more dispersed system, indicating reduced compactness, while a lower Rg value indicates a more condensed and closely packed system (Senthilkumar & Rajasekaran, 2017; Sharma et al., 2019). When comparing the Radius of Gyration between two variables, it is essential to consider their specific attributes and functions within the system. Through this comparison, scientists can discern insights into the relative impacts and contributions of different variables to the system's size and compactness. This process aids in comprehending the overall shape and distribution of the system's constituents.

Figure 5 illustrates the profile of the radius of gyration for protein-ligand complexes. The mean of the dependent variable for 4-thiouridine is 2.368125, whereas for β-D-glucopyranose, it is 2.36011. This indicates that, on average, the radius of gyration for 4-thiouridine is marginally larger than that for β-D-glucopyranose. Upon reviewing the standard deviations, the dependent variable for 4-thiouridine has a standard deviation of 0.004238056, while β-D-glucopyranose has a standard deviation of 0.003985518. This suggests that fluctuations in the radius of gyration for 4-thiouridine are slightly more pronounced compared to those for β-D-glucopyranose. The comparison of the radius of gyration results from molecular dynamics simulations between 4-thiouridine and β-D-glucopyranose yields intriguing insights. On average, 4-thiouridine exhibits a slightly larger radius of gyration compared to β-D-glucopyranose. Additionally, fluctuations in the radius of gyration for 4-thiouridine are slightly more pronounced than those for β-D-glucopyranose. Analyzing the results for β-D-xylopyranose and α-D-xylopyranose in molecular dynamics simulations, it becomes evident that β-D-xylopyranose displays a slightly larger average value, increased variability, and more substantial fluctuations compared to α-D-xylopyranose.

Solvent Accessible Surface Area (SASA) is a metric employed in molecular dynamics simulations to evaluate the surface area accessible to solvent molecules for a molecule or a specific region. This measurement offers crucial insights into the exposure of atoms or particles to the surrounding solvent environment, contributing to an understanding of molecular interactions, ligand binding, and protein folding. SASA is determined by considering the positions of atoms or particles and the radius of a solvent molecule, ultimately defining the surface area accessible to solvent molecules during their interaction with the system. When comparing the SASA of two distinct variables, it is essential to account for their specific attributes and roles within the system. Such a comparison enables researchers to assess their relative solvent accessibility, drawing inferences about their distinct interactions with the surrounding solvent environment. This provides valuable insights into the roles and behaviors of these variables within the molecular system.

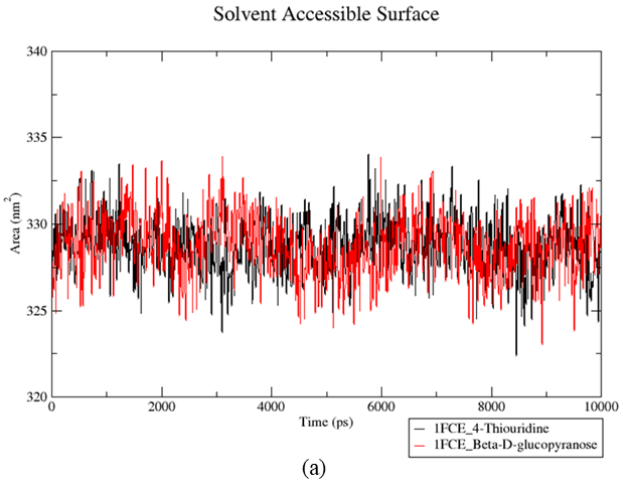

(a)

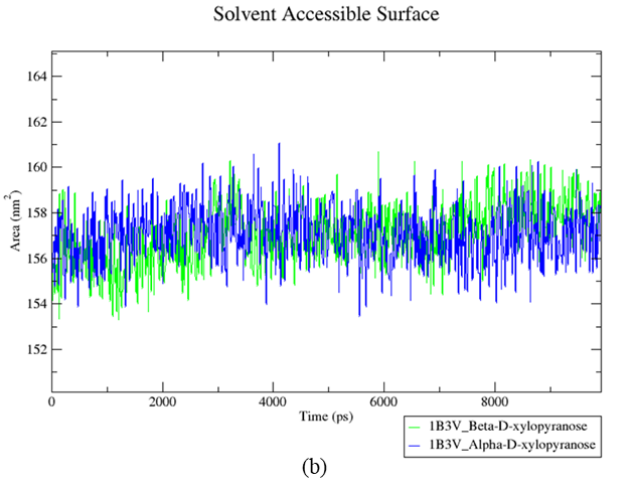

(b)

Figure 6. Solvent Accessible Surface Area (SASA) of xylanase – ligand complexes from molecular dynamic simulation.

The comparative analysis of Solvent Accessible Surface Area (SASA) outcomes from molecular dynamics simulations between 4-thiouridine and β-D-glucopyranose yields insights into their respective characteristics (Figure 6). The mean value of the dependent variable for 4-thiouridine is 328.7648, while for β-D-glucopyranose, it is 328.7752. This implies that both molecules exhibit similar average values for the SASA. Examining the standard deviations reveals that 4-thiouridine has a standard deviation of 1.627079, while β-D-glucopyranose has a standard deviation of 1.732647. This indicates that the fluctuations in the SASA for both molecules are relatively alike and display comparable variability. The regression coefficients offer insights into the relationship between the independent and dependent variables. For 4-thiouridine, the regression coefficient (slope) is –5.181474e-005, signifying a slight decrease in the dependent variable for each unit increase in the independent variable. Similarly, β-D-glucopyranose has a regression coefficient of –7.258963e-005, indicating a slightly more substantial decrease in the dependent variable for each unit increase in the independent variable. The t-values associated with the coefficients indicate their statistical significance.

The mean value of the dependent variable for α-D-xylopyranose is 157.1041, while for β-D-xylopyranose, it is 157.0879. This implies that both molecules showcase similar average values for the SASA. Upon scrutinizing the standard deviations, β-D-xylopyranose exhibits a standard deviation of 1.289849, while α-D-xylopyranose has a standard deviation of 1.154096. This suggests that the fluctuations in the SASA for both molecules are relatively alike, although β-D-xylopyranose displays slightly higher variability compared to α-D-xylopyranose. Assessing the correlation coefficients, β-D-xylopyranose demonstrates a positive correlation of 0.526893 with the independent variable, indicating a moderately positive relationship between the variables. Conversely, α-D-xylopyranose exhibits a very weak positive correlation of 0.001532941, suggesting an almost negligible relationship between the variables. The regression coefficients offer insights into the relationship between the independent and dependent variables. For β-D-xylopyranose, the regression coefficient (slope) is 0.000235072, indicating a minor increase in the dependent variable for each unit increase in the independent variable. In contrast, α-D-xylopyranose has a regression coefficient of 6.119378e-007, suggesting an almost inconsequential increase in the dependent variable for each unit increase in the independent variable. These findings contribute valuable insights into the characteristics and dynamics of the two variables within the molecular systems under investigation.

CONCLUSION

Xylanase, an enzyme specialized in degrading xylan, holds significant industrial advantages. Understanding the structure of xylan and its interactions with ligands plays a crucial role in comprehending enzyme characteristics and enhancing enzyme performance. Xylanase from *Penicillium simplicissimum* (PDB 1B3V) and *Clostridium cellulolyticum* (PDB 1FCE) offers insights into the interactions between xylanase and ligands, shedding light on the stability within this interplay. The binding energies between fungal xylanase (PDB 1B3V) and α-D-xylopyranose, as well as β-D-xylopyranose, are –5.6 kcal/mol and –5.5 kcal/mol, respectively.

Bacterial xylanase (PDB 1FCE) exhibits binding energies of –5.7 kcal/mol toward 4-thiouridine and –5.9 kcal/mol toward β-D-glucopyranose. This research provides new insights into the structural and molecular dynamics of fungal and bacterial xylanase when interacting with ligands.

ACKNOWLEDGMENT

The authors would like to appreciate to Laboratory of Enzyme Technology & Biomaterials, Faculty of Mathematics and Natural Sciences, Universitas Lambung Mangkurat for supporting the research activity and facilities. This work was supported by Universitas Lambung Mangkurat to Noer Komari and Rahmat Eko Sanjaya (Program Dosen Wajib Meneliti, Rector Decree No. 615/UN8/PG/2023).

REFERENCES

Abraham, M. J., Murtola, T., Schulz, R., Páll, S., Smith, J. C., Hess, B., & Lindah, E. (2015). Gromacs: High performance molecular simulations through multi-level parallelism from laptops to supercomputers. *SoftwareX*, *1–2*, 19–25.

Allen, W. J., Balius, T. E., Mukherjee, S., Brozell, S. R., Moustakas, D. T., Lang, P. T., Case, D. A., Kuntz, I. D., & Rizzo, R. C. (2015). DOCK 6: Impact of New Features and Current Docking Performance. *Journal of Computational Chemistry*, *36*(15), 1132.

Annadurai, Y., Balasubramanian, B., Arumugam, V. A., Liu, W., Pushparaj, K., Pappusamy, M., Kuchi Bhotla, H., Meyyazhagan, A., Easwaran, M., & Piramanayagam, S. (2021). Comprehensive strategies of Lignocellulolytic enzyme production from microbes and their applications in various commercial-scale faculties. *Natural Resources for Human Health*, *2*(1), 1–31.

Bhalla, A., Bischoff, K. M., & Sani, R. K. (2014). Highly thermostable GH39 β-xylosidase from a Geobacillus sp. strain WSUCF1. *BMC Biotechnology*, *14*(1), 963.

Cole, J. C., Murray, C. W., Nissink, J. W. M., Taylor, R. D., & Taylor, R. (2005). Comparing protein–ligand docking programs is difficult. *Proteins: Structure, Function, and Bioinformatics*, *60*(3), 325–332.

Danova, A., Maulana, Y. E., Hermawati, E., & Chavasiri, W. (2023). Synthesis, Evaluation, and Molecular Docking Study of 4-Monoacyl Resorcinol Against Tyrosinase Enzyme. *Indo. J. Chem. Res.*, *11*(2), 135–141.

Den Haan, R., & Van Zyl, W. H. (2003). Enhanced xylan degradation and utilisation by Pichia stipitis overproducing fungal xylanolytic enzymes. *Enzyme and Microbial Technology*, *33*(5), 620–628.

Dos Reis, S., Ferreira Costa, M. A., & Peralta, R. M. (2003). Xylanase production by a wild strain of Aspergillus nidulans. *Acta Scientiarum - Biological Sciences*, *25*(1), 221–225.

Fitriana, A. S., & Royani, S. (2022). Molecular Docking Study of Chalcone Derivatives as Potential Inhibitors of SARS-CoV-2 Main Protease. *Indo. J. Chem. Res.*, *9*(3), 150–162.

Fu, Y., Zhao, J., & Chen, Z. (2018). Insights into the molecular mechanisms of protein-ligand interactions by molecular docking and molecular dynamics simulation: A case of oligopeptide binding protein. *Computational and Mathematical Methods in Medicine*, *2018*, 1–12.

Gaspersz, N., & Sohilait, M. R. (2019). Penambatan Molekuler α, β, dan γ-mangostin Sebagai Inhibitor α-amilase Pankreas Manusia. *Indo. J. Chem. Res.*, *6*(2), 59–66.

Gyebi, G. A., Ogunyemi, O. M., Ibrahim, I. M., Ogunro, O. B., Adegunloye, A. P., & Afolabi, S. O. (2021). SARS-CoV-2 host cell entry: an in silico investigation of potential inhibitory roles of terpenoids. *Journal of Genetic Engineering and Biotechnology 2021 19:1*, *19*(1), 1–22.

Javed, U., Aman, A., & Qader, S. A. U. (2017). Utilization of corncob xylan as a sole carbon source for the biosynthesis of endo-1,4-β xylanase from Aspergillus niger KIBGE-IB36. *Bioresources and Bioprocessing*, *4*(1), 1–7.

Mathur, N., Goswami, G. K., & Pathak, A. N. (2017). Structural comparison, docking and substrate interaction study of modeled endo-1, 4-beta xylanase enzyme of Bacillus brevis. *Journal of Molecular Graphics and Modelling*, *74*, 337–343.

Mulyati, B., & Seulina Panjaitan, R. (2021). Study of Molecular Docking of Alkaloid Derivative Compounds from Stem Karamunting (Rhodomyrtus tomentosa)Against α-Glucosidase Enzymes. *Indo. J. Chem. Res*, *9*(2), 129–136.

Nair, S. G., & Shashidhar, S. (2008). Fungal xylanase production under solid state and submerged fermentation conditions. *African Journal of Microbiology Research*, *2*(4), 82–86.

Parab, P., & Khandeparker, R. (2021). Xylanolytic enzyme consortia from Bacillus sp. NIORKP76

for improved biobleaching of kraft pulp. *Bioprocess and Biosystems Engineering*, *44*(12), 2513–2524. https://doi.org/10.1007/s00449-021-02623-6

Patel, A. K., Singhania, R. R., Sim, S. J., & Pandey, A. (2019). Thermostable cellulases: Current status and perspectives. *Bioresource Technology*, *279*(November 2018), 385–392.

Polizeli, M. L. T. M., Rizzatti, A. C. S., Monti, R., Terenzi, H. F., Jorge, J. A., & Amorim, D. S. (2005). Xylanases from fungi: Properties and industrial applications. *Applied Microbiology and Biotechnology*, *67*(5), 577–591.

Ramos, M. D. N., Rangel, A. S., Azevedo, K. S., Melo, M. G. B., Oliveira, M. C., Watanabe, C. M. U., Pereira, F. F., Silva, C. M., & Aguiar, A. (2022). Characteristics and treatment of Brazilian pulp and paper mill effluents: a review. *Environmental Monitoring and Assessment*, *194*(9), 651.

Rashid, W. B. A. B., Abd Malek, R., Wadaan, M. A., Elsayed, E. A., Sukmawati, D., & El-Enshasy, H. A. (2020). Medium optimization for xylanase production by recombinant Escherichia coli B24. *Journal of Scientific and Industrial Research*, *79*(6), 473–478.

Rusli, F. M., Mohamed, M. S., Mohamad, R., Puspaningsih, N. N. T., & Ariff, A. B. (2009). Kinetics of Xylanase Fermentation by Recombinant Escherichia coli DH5α in Shake Flask Culture. *American Journal of Biochemistry and Biotechnology*, *5*(3), 110–118.

Safitri, E., Hanifah, Previta, Sudarko, Tri Puspaningsih, N. N., & Istri Ratnadewi, A. A. (2021). Cloning, purification, and characterization of recombinant endo- β-1,4-D-xylanase of Bacillus sp. From soil termite abdomen. *Biocatalysis and Agricultural Biotechnology*, *31*(November 2020), 101877.

Saha, B. C. (2003). Hemicellulose bioconversion. *Journal of Industrial Microbiology and Biotechnology*, *30*(5), 279–291.

Senthilkumar, B., & Rajasekaran, R. (2017). In Silico Template Selection of Short Antimicrobial Peptide Viscotoxin for Improving Its Antimicrobial Efficiency in Development of Potential Therapeutic Drugs. *Applied Biochemistry and Biotechnology*, *181*(3), 898–913.

Sharma, K., Thakur, A., Kumar, R., & Goyal, A. (2019). Structure and biochemical characterization of glucose tolerant β-1,4 glucosidase (HtBgl) of family 1 glycoside hydrolase from Hungateiclostridium thermocellum. *Carbohydrate Research*, *483*.

Sürmelı, Y. (2023). In Silico Phylogeny, Sequence and Structure Analyses of Fungal Thermoacidophilic GH11 Xylanases. *Journal of Tekirdag Agricultural Faculty*, *20*(1), 211–229.

Swain, M. R., & Krishnan, C. (2015). Improved conversion of rice straw to ethanol and xylitol by combination of moderate temperature ammonia pretreatment and sequential fermentation using Candida tropicalis. *Industrial Crops and Products*, *77*, 1039–1046.

Terrasan, C. R. F., Temer, B., Sarto, C., Silva Júnior, F. G., & Carmona, E. C. (2013). Xylanase and β-Xylosidase from Penicillium janczewskii: Production, Physico-Chemical properties, and application of the crude extract to pulp biobleaching. *BioResources*, *8*(1), 1292–1305.

Wong, K. K., Tan, L. U., & Saddler, J. N. (1988). Multiplicity of beta-1,4-xylanase in microorganisms: functions and applications. *Microbiological Reviews*, *52*(3), 305–317.

Yang, J., & Han, Z. (2018). Understanding the positional binding and substrate interaction of a highly thermostable GH10 xylanase from thermotoga maritima by molecular docking. *Biomolecules*, *8*(3).